Electronic Supplementary Material (ESI) for Nanoscale.

INTER-PARTICLE BIOMOLECULAR REACTIVITY TUNED BY SURFACE CROWDERS

M.R.W. Scheepers[1,3], S.R.R. Haenen[1], J.M. Coers[1], L.J. van IJzendoorn[1,3], M.W.J. Prins[1,2,3,*]

[1]Eindhoven University of Technology, Department of Applied Physics, PO Box 513, 5600 MB Eindhoven, The Netherlands
[2]Eindhoven University of Technology, Department of Biomedical Engineering, PO Box 513, 5600 MB Eindhoven, The Netherlands
[3]Eindhoven University of Technology, Institute for Complex Molecular Systems, PO Box 513, 5600 MB Eindhoven, The Netherlands
*m.w.j.prins@tue.nl

SUPPORTING INFORMATION

- 11 pages
- 5 figures
- 4 tables

S1) Optomagnetic cluster (OMC) experiment

In this paper specific particle aggregation rates are measured using the OMC experiment described in a previous paper[21]. Fig. S1a sketches the optomagnetic cluster (OMC) experiment. A square glass cuvette filled with a solution of particles is situated in the centre of a quadrupole electromagnet setup, which produces a rotating magnetic field in the y,z plane. A 660 nm laser is focussed insight the cuvette and the light scattered by the particles is measured by a photodetector at an angle of 90° w.r.t. to the incoming laser beam. In the presence of a rotating magnetic field, with a rotation frequency below the breakdown frequency, the dimers in the solution rotate synchronously with the magnetic field.

Fig. S1c shows the oscillating scattering signal for both types of superparamagnetic particles used in this paper: polystyrene Ademtech Masterbeads (d = 528 nm, CV ≈ 25%) and silica Microparticles (d = 511 nm, CV < 5%). The differences in the scattering signals of Ademtech and Microparticle dimers are caused by differences in refractive index, size and size dispersion. For example, the oscillating scattering signal of the Microparticles contains more peaks compared to the Ademtech signal, although the particle size is very similar. However, due to the large size dispersion of the Ademtech particles the measured scattering signal is the average of many dimers consisting of particles with different sizes, whereby detailed features of the scattering signal are lost. Note that even in case the size dispersion of Ademtech and Microparticles would have been equal, the scattering signals would differ due to the different refractive indices of the particles ($n_{Ademtech}$ = 1.83$\pm$0.08, $n_{Microparticles}$ = 1.59$\pm$0.04).

The amplitude of the oscillating scattering signal is a measure of the amount of dimers that are present in the solution. Therefore, the Fourier transform of the scattering signals of Fig. S1c is shown in Fig. S1d. Several peaks are observed at frequencies that are multiples of two times the field rotation frequency f_{rot} = 5 Hz. The peak at the frequency equal to four times the field rotation frequency, |A4f|, is used as a measure of the dimer concentration. Fig. S1e shows a calibration measurement of the |A4f| as a function of the concentration of a particle stock solution. In these stock solutions a certain fraction of the particles is in dimer form (1 in 12 for Ademtech, 1 in 9 for Microparticles) which leads to a measurable |A4f| peak. By diluting the stock solution several times, the dimer concentration is varied and the |A4f| is measured. The slopes of the fitted curves in the loglog plot being about equal to 1 indicate a linear relation between |A4f| and dimer concentration for both particle types. Fig. S1f shows a single actuation cycle that is used to quantify the aggregation rate for both particle types. Both panels show a constant |A4f| throughout the measurement phases and a rather linearly increasing |A4f| during the actuation phase.

To quantify the aggregation rate a four-step actuation protocol is followed, as can be seen in Fig. S1b. Initially the number of already present chemical dimers is measured using magnetic pulses with a short on-time, t_{on} = 0.4 s, and a long off time, t_{off} = 10 s. During the subsequent actuation phase, the rotating magnetic field is turned on continuously during a time t_{act} = 20 s to induce additional magnetic dimers, causing the |A4f| signal to increase approximately linearly over time (this is true for both types of particles, see Fig. S1f). Since each magnetic dimer is formed at a different point in time, each magnetic dimer has a different interaction time in which it has the possibility to form a chemical bond. The mean interaction time of all dimers, for a constant magnetic dimer formation rate, equals half the actuation time. After the actuation phase, the field is turned off during a waiting time t_{wait} = 80 s to let the non-aggregated particles redisperse in solution. Ultimately, the number of chemical dimers is measured again and compared to the initial number of dimers. The increase in the number of chemical dimers, ΔN_{chem}, depends on how reactive the particles are. To calculate the aggregation rate k_{agg}^{mag}, the fraction of magnetic dimers that becomes a chemical dimer during the actuation phase, $\Delta N_{chem}/N_{mag,tot}$, is divided by the mean interaction time of all magnetic dimers.

$$k_{agg} = \frac{\Delta N_{chem} \,/\, N_{mag,tot}}{\frac{1}{2} t_{act}} \qquad \text{(S1)}$$

In case of very reactive particles, it is possible that all magnetic dimers form a chemical bond during the interaction time. For a 20 s actuation time the maximum experimentally measurable aggregation rate is limited to $k_{agg,max}^{mag}$ = 0.1 s^{-1}.

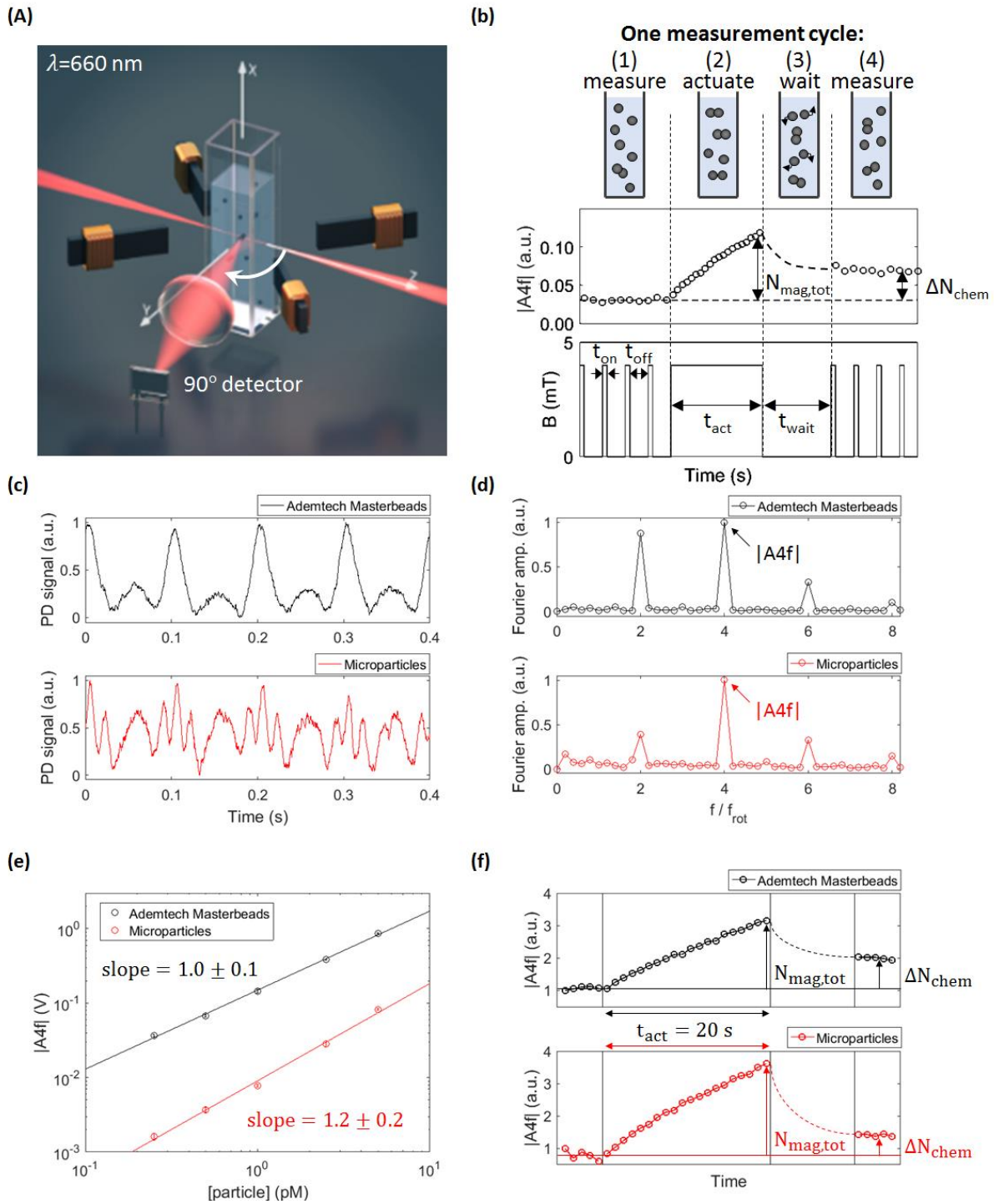

Fig. S1 ***Optomagnetic cluster experiment*** *(a) Optomagnetic dimer quantification: A 660 nm laser is focussed inside a cuvette filled with a particle solution. The scattering of the particles is measured at an angle of 90° w.r.t. the incoming laser beam. Four electromagnets are placed around the cuvette to apply a rotating magnetic field. Particle dimers are rotated, which leads to an oscillating scattering signal. The amplitude of the oscillating signal is used as measure of the dimer*

concentration. (b) Four-step actuation protocol to quantify the aggregation rate. First, the initial number of chemical dimers in the solution is measured using short magnetic field pulses. Then the field is turned on continuously to induce additional magnetic dimers, during an actuation time t_{act}. The field is subsequently turned off for a waiting time t_{wait} to let the unbound particles redistribute in the solution. Finally, the new number of chemical dimers is measured. Using equation 2 the aggregation rate can be determined. (c) Oscillating scattering signal of both types of superparamagnetic particles, Ademtech Masterbeads and Microparticles, measured by a photodetector at an angle of 90° w.r.t. the incoming laser beam in the presence of a rotating magnetic field, f_{rot} = 5 Hz. (d) Fourier transform of the oscillating scattering signals of Fig. S1c, showing peaks at multiples of two times the field rotation frequency. (e) Calibration measurement of |A4f| as a function of particle concentration of a stock solution (containing a constant number of dimers), indicating that the |A4f| scales linearly with dimer concentration. (f) Single actuation cycle to measure the aggregation rate with the OMC experiment, for both particle types.

S2) List of used DNA strands

In this paper three different DNA constructs are used: A functional docking strand, a DNA filler strand and an analyte strand. These double stranded DNA constructs are built up from the five single stranded DNA sequences shown in Table S2. The DNA docking strand is obtained by annealing the base strand B with the docking strand D. The DNA filler strand is obtained by annealing the base strand B with the filler strand F. The analyte construct is obtained by annealing the analyte strand 1 with the analyte strand 2.

Table S2 Single stranded DNA sequences for DNA model system *Overview of the single stranded DNA sequences from which the DNA docking strand (B+D), the DNA filler strand (B+F) and the DNA analyte strand (A1+A2) are made of.*

Code:	Name:	Sequence:
B	base strand	biotin-5'-CCT CCC AGC CCA TCC TAA CC-3'
F	filler strand	3'-GGA GGG TCG GGT AGG ATT GG-5'
D	docking strand	3'-GGA GGG TCG GGT AGG ATT GG AAG CAG CAG AAC AAA-5'
A1	analyte strand 1	5'-TTC GTC GTC TTG TTT CCA CCC TTC CCG CCC CTC CC-3'
A2	analyte strand 2	5'-TTC GTC GTC TTG TTT GGG AGG GGC GGG AAG GGT GG-3'

S3) Supernatant assay for DNA docking strand density quantification

To determine the maximum DNA coverage of the streptavidin coated Microparticles for short biotinylated DNA strands, an indirect fluorescence supernatant assay is performed. Fig. S2a shows in blue a calibration curve of the fluorescence intensity corresponding to concentration of biotin-atto655. The capacity of the Microparticles for b-atto655 is measured by incubating different b-atto655 concentrations with a constant particle concentration. After 60 minutes of incubation in an incubator shaker (1200 rpm, room temperature), the fluorescence of the supernatant is measured (green line in Fig. S3a). The b-atto655 capacity per particle is obtained from the point in the graph where the fluorescence intensity of the supernatant starts increasing, $N_{b-atto655}$ = (4.3±0.5)·10^4. The measured capacity is slightly lower than the geometrical capacity that can be expected based on the size of the particle (d = 511 nm), the size of a streptavidin (sphere, $d \sim 5$ nm) and the number of functional biotin binding pockets per streptavidin (~2.5 out of 4), see Fig. S3a.

In the indirect supernatant assay the particles are first functionalized with different amounts of biotinylated DNA strands for 60 minutes in an incubator shaker (1200 rpm, room temperature). Subsequently particles are magnetically washed and another incubation step is performed with a b-atto655 concentration that is slightly higher than the b-atto655 capacity. From the fluorescence intensity of the supernatant, the DNA coverage can be calculated using equation 1. Fig. S3b shows that when increasing the DNA concentration the DNA coverage also increases, until a plateau is reached at $N_{dock,max}$ = (1.6±0.3)·10^4. The corresponding maximum docking strand coverage is $\sigma_{dock,max}$ = (2.0±0.4)·10^4 µm^{-2}. The DNA capacity is about a factor three lower than the b-atto655 capacity, which can most likely be explained by the negative charge on the DNA backbone.

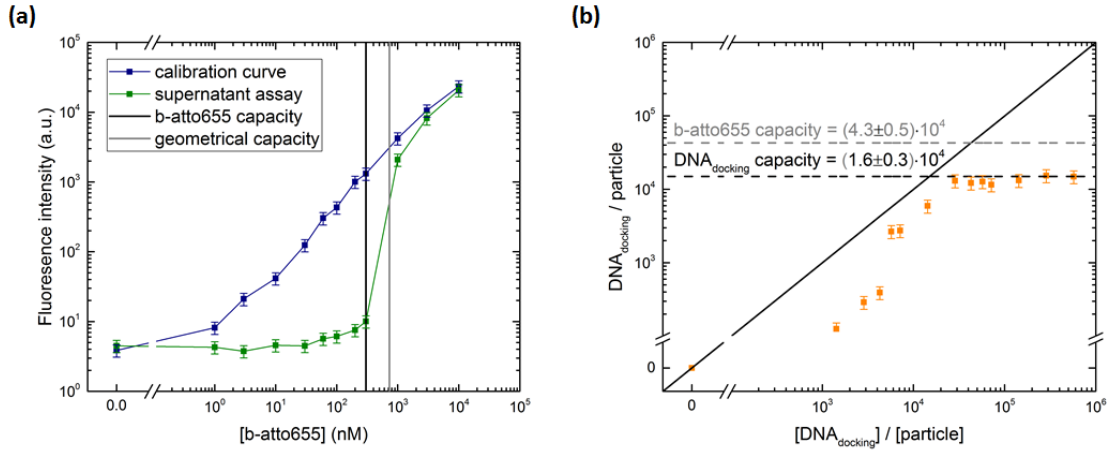

Fig. S3 Supernatant assay for DNA docking strand quantification *(a) Calibration curve (blue) of the fluorescence intensity as a function of the biotin-atto655 concentration. Supernatant assay (green) after b-atto655 incubation with streptavidin coated Microparticles to obtain the capacity of the particles for b-atto655. (b) DNA coverage per particle as a function of the DNA concentration during incubation, measured with an indirect fluorescence supernatant assay.*

S4) Antibody sandwich system: control experiment

To investigate whether the aggregation in the antibody sandwich system is specific and originates from the antibody sandwich, a control experiment was performed. Two batches of particles were functionalized: One batch coated with only αPSA10 antibodies and one batch coated with only αPSA66 antibodies. Fig. S4 shows the aggregation rate that was measured with the OMC experiment, using either a mixture of both particles (blue data points) or only particles coated with αPSA10 (green data points). For the mixture of particles a clear increase in the aggregation rate is observed as a function of the [PSA] to [particle] ratio. For the control experiment with only αPSA10 coated particles no response is observed for increasing [PSA] to [particle] ratio.

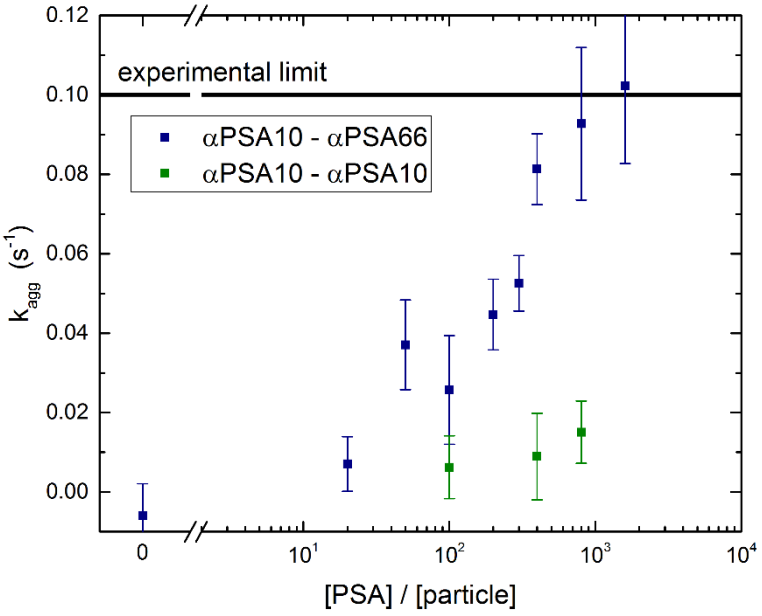

Fig. S4 Control experiment for antibody sandwich system *Aggregation rate is measured for a mixture of particles coated with αPSA10 and particles coated with αPSA66 (blue) and a control experiment where only particles are used with αPSA10 (green).*

S5) Simulation parameter scan

A parameter scan of the input parameters of the aggregation simulation has been performed to investigate the effect of each parameter on the simulated aggregation rate. Table S5 shows the default input values of the simulation during the parameter scan. While one parameter is scanned, the other parameters are constant and equal to the default values. Some parameters are not scanned: particle radius R, maximum bond length L_{bond} and incubation time t_{inc}.

Table S5 Default values input parameters of simulation *Overview of the default values of the input parameters that are used in the parameter scan of the aggregation rate simulations.*

default input values parameter scan			
parameter	**symbol**	**value**	**unit**
particle radius	R	0.25	µm
maximum bond length	L_{bond}	0.027	µm
interparticle distance	Δx	0.019	µm
incubation time	t_{inc}	360	s
analyte association rate	k_{on}	10^6	$M^{-1}s^{-1}$
actuation time	t_{act}	20	s
magnetic dimer formation rate	k_{enc}^{mag}	10^3	s^{-1}
chemical aggregation rate	k_{chem}	$2 \cdot 10^{-6}$	$\mu m^2 s^{-1}$
nonspecific chemical aggregation rate	$k_{chem,ns}$	0	s^{-1}
binder surface density	σ_B	$5.1 \cdot 10^3$	μm^{-2}

Fig. S5a shows the parameter scan for the binder surface density σ_B. For increasing binder density the aggregation rate curve shifts upward to higher rates, as more binders leads to more options to form bonds between the particles. Fig. S5b shows the parameter scan for the magnetic encounter rate k_{enc}^{mag}. The aggregation process does not depend on the encounter rate, but for higher encounter rates, the statistics increases and thus the fluctuations decrease. Fig. S5c shows the parameter scan for the actuation time t_{act}. For increasing actuation times the probability that a dimer aggregates is larger. This leads to a higher aggregation rate. However, for very reactive dimers, i.e. when the typical time-to-aggregation is smaller than the mean interaction time, the aggregation rate is underestimated. This underestimation is greater for the longer actuation times compared to the shorter actuation times. Therefore the curves intersect around their peak values. Fig. S5d shows the parameter scan for the nonspecific aggregation rate. For nonzero nonspecific aggregation rate a baseline of the simulated aggregation rate is observed. For increasing nonspecific aggregation rates, this baseline level shifts upwards to higher aggregation rates.

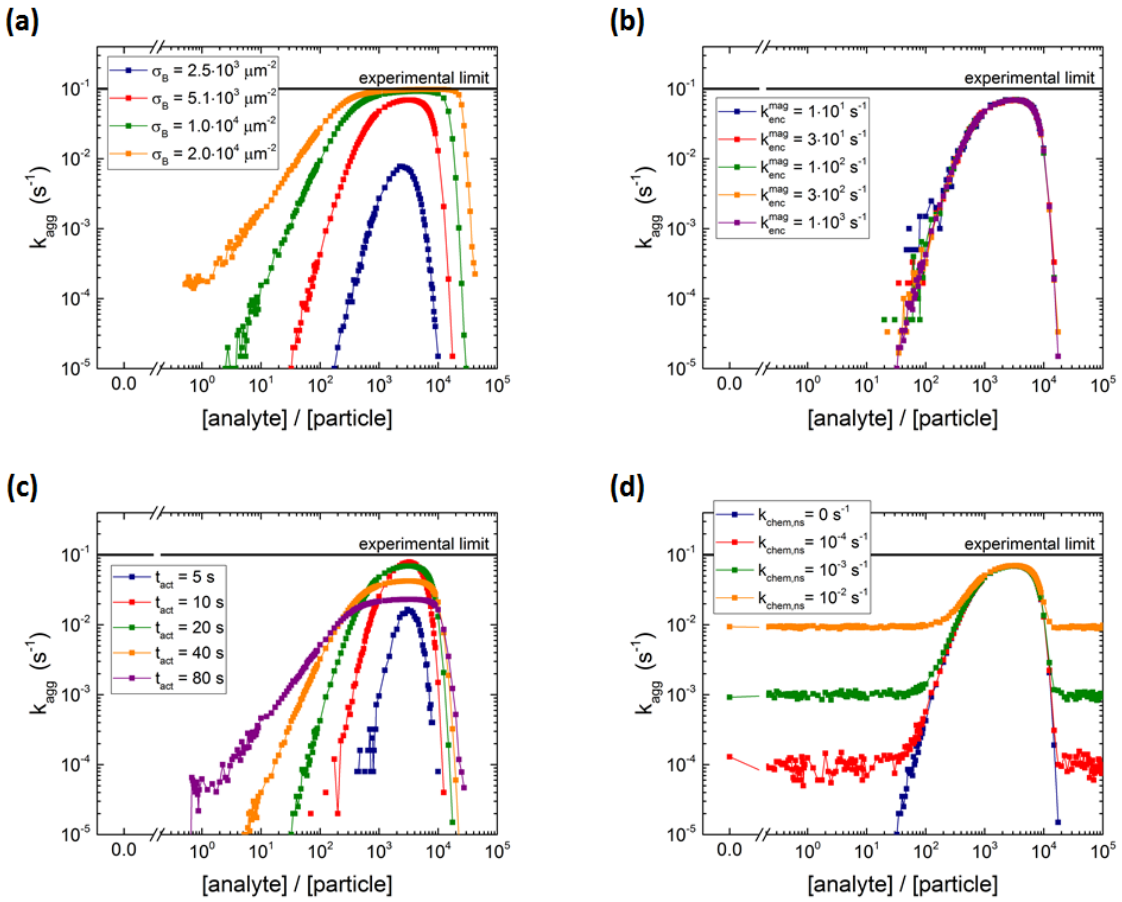

Fig. S5 Parameter scan of aggregation simulation *(a) Simulated aggregation rate as a function of the analyte-to-particle ratio for the parameter scan of the binder surface density σ_B. Increasing binder density leads to increasing aggregation rate for every analyte concentration, i.e. the curve shifts upwards. (b) Parameter scan of the magnetic dimer formation rate k_{enc}^{mag}. Changing the rate at which magnetic dimers are formed does not change the aggregation process, though it determines the statistical fluctuations in the simulation. (c) Parameter scan of the actuation time. For increasing actuation time, the mean interaction time will increase, and therefore the aggregation rate will increase. However, the maximum measurable aggregation rate decreases for increasing actuation time, which leads to a lower peak of the curve for increasing actuation times. (d) Parameter scan of the nonspecific chemical aggregation rate $k_{chem,ns}$. For increasing nonspecific aggregation rate the background aggregation level increases.*

S6) Input parameter for simulation of varying binder density

The input parameters used for the simulated curves shown in Fig. 2b and 2d are shown in Table S6. The particle radius R, the incubation time t_{inc}, the actuation time t_{act} and the magnetic encounter rate k_{enc}^{mag} have equal values for the DNA model system and the antibody sandwich system. The bond length L_{bond}, interparticle distance Δx, the association rate k_{on}, the specific chemical aggregation rate k_{chem} and the nonspecific chemical aggregation rate $k_{chem,ns}$ are different for the two experimental systems, but they are constant throughout the simulations. The binder density on the particle surface σ_B is varied experimentally and therefore also varied in the simulations.

Table S6 Simulation input parameters: *Overview of the parameters that are used in the simulation to match to the experimental results of Fig. 1d and Fig. 1f.*

DNA model system			Antibody sandwich system		
parameter	**value**	**unit**	**parameter**	**value**	**unit**
R	0.25	µm	R	0.25	µm
L_{bond}	0.031	µm	L_{bond}	0.035	µm
Δx	0.019	µm	Δx	0.019	µm
t_{inc}	360	s	t_{inc}	360	s
k_{on}	$1.5 \cdot 10^6$	$M^{-1}s^{-1}$	k_{on}	$1.9 \cdot 10^5$	$M^{-1}s^{-1}$
t_{act}	20	s	t_{act}	20	s
k_{enc}^{mag}	10^2	s^{-1}	k_{enc}^{mag}	10^2	s^{-1}
k_{chem}	$5.0 \cdot 10^{-4}$	$\mu m^2 s^{-1}$	k_{chem}	$9.5 \cdot 10^{-6}$	$\mu m^2 s^{-1}$
$k_{chem,ns}$	0.005	s^{-1}	$k_{chem,ns}$	0.005	s^{-1}
σ_B	$1.3 \cdot 10^2$ $2.5 \cdot 10^2$ $5.1 \cdot 10^2$ $2.0 \cdot 10^4$	μm^{-2}	σ_B	$7.6 \cdot 10^3$ $(45.0 \frac{\mu g}{mL})$ $3.8 \cdot 10^3$ $\left(22.5 \frac{\mu g}{mL}\right)$ $1.0 \cdot 10^3$ $\left(11.3 \frac{\mu g}{mL}\right)$	μm^{-2}

S7) Association rate dependence for high docking strand coverage

Fig. S7 shows the experimental data for high docking strand coverage σ_{dock} = 2.0·10^4 µm^{-2}. The data is accompanied with two simulations using the input parameters of Table S6 and an association rate of either k_{on} = 1.5·10^6 M^{-1}s^{-1} and k_{on} = 1.0·10^5 M^{-1}s^{-1}. The experimental data agrees best with the association rate k_{on} = 1.0·10^5 M^{-1}s^{-1}, whereas the for the lower docking strand coverages in Fig. 2b the data agrees best with k_{on} = 1.5·10^6 M^{-1}s^{-1}. The lower association rate at higher docking strand density might be explained by the fact that there is much more DNA bound at the surface of the particles which has a repulsive electrostatic effect.

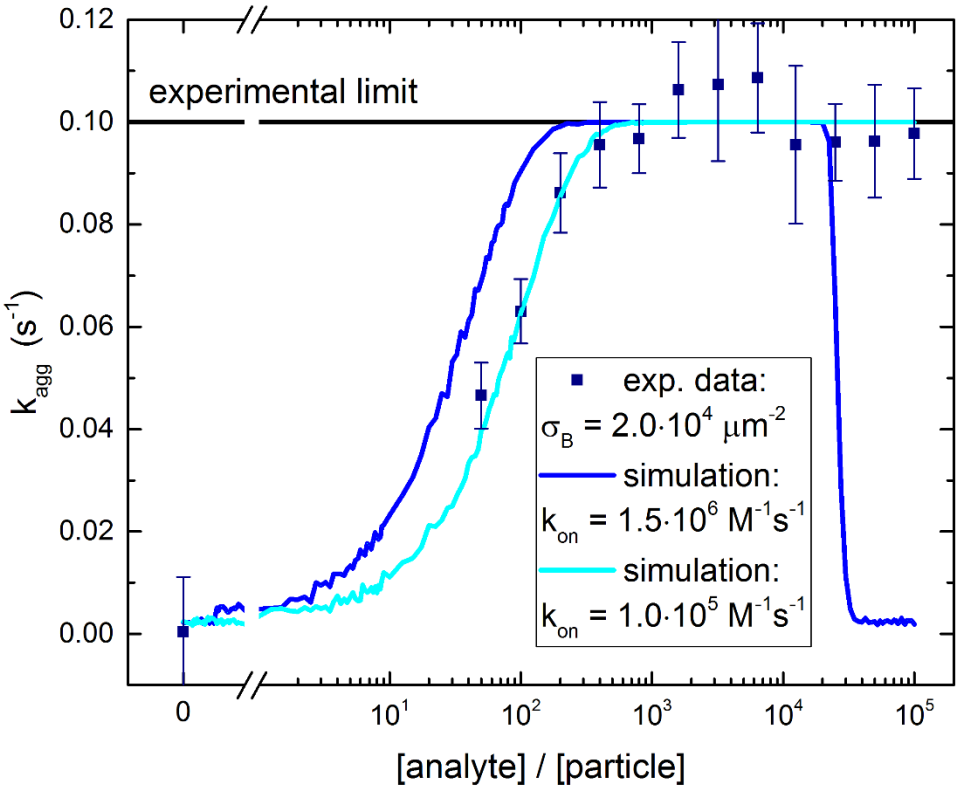

Fig. S7 Lower association rate for high docking strand density *Measured aggregation rate for the DNA model system with a DNA docking strand density σ_{dock} = 2.0·10^4 µm^{-2}. The experimental data is accompanied with two simulated curves having analyte association rate k_{on} = 1.5·10^6 M^{-1}s^{-1} and k_{on} = 1.0·10^5 M^{-1}s^{-1}.*

S8) Input parameter for simulation of varying PEG molecular weight

The input parameters used for the simulated curves shown in Fig. 4c and 4f are shown in Table S8. The particle radius R, the incubation time t_{inc}, the actuation time t_{act} and the magnetic encounter rate k_{enc}^{mag} have equal values for the DNA model system and the antibody sandwich system. The bond length L_{bond}, interparticle distance Δx, the association rate k_{on} and the nonspecific chemical aggregation rate $k_{chem,ns}$ are different for the two experimental systems. The specific molecular binding rate k_{chem} is varied in the simulation to reproduce the experimental results in the presence of a PEG coating.

Table S8 Simulation input parameters: *Overview of the parameters that are used in the simulation to match to the experimental results of Fig. 4c and Fig. 4f.*

DNA model system			Antibody sandwich system		
parameter	**value**	**unit**	**parameter**	**value**	**unit**
R	0.25	µm	R	0.25	µm
L_{bond}	0.031	µm	L_{bond}	0.035	µm
Δx	0.019	µm	Δx	0.019	µm
t_{inc}	360	s	t_{inc}	360	s
k_{on}	$1.5 \cdot 10^5$	$M^{-1}s^{-1}$	k_{on}	$1.9 \cdot 10^5$	$M^{-1}s^{-1}$
t_{act}	20	s	t_{act}	20	S
k_{enc}^{mag}	10^2	s^{-1}	k_{enc}^{mag}	10^2	s^{-1}
k_{chem}	**low MW PEG** $5.0 \cdot 10^{-4}$ **high MW PEG** $6.5 \cdot 10^{-7}$	$\mu m^2 s^{-1}$	k_{chem}	**low MW PEG** $9.5 \cdot 10^{-6}$ **high MW PEG** $1.4 \cdot 10^{-6}$	$\mu m^2 s^{-1}$
$k_{chem,ns}$	**low MW PEG** 0.03 **high MW PEG** 0.005	s^{-1}	$k_{chem,ns}$	**low MW PEG** 0.005 **high MW PEG** 0.005	s^{-1}
σ_B	$5.6 \cdot 10^3$	μm^{-2}	σ_B	$3.8 \cdot 10^3$	μm^{-2}